American Mineralogist, Volume 79, pages 700–711, 1994

Morphological characteristics of illitic clay minerals from a hydrothermal system

Atsuyuki Inoue
Geological Institute, College of Arts and Sciences, Chiba University, Chiba 263, Japan
Ryuji Kitagawa
Institute of Geology and Mineralogy, Hiroshima University, Higashi-Hiroshima 724, Japan

Abstract

Variations in the morphology of illitic clay minerals were observed in the Kamikita hydrothermal system for illitized smectite. Particle sizes and microtopographies were measured by transmission electron microscopy using Pt shadowing and Au decoration. Particle size distributions normalized to the modes gave steady-state profiles skewing toward larger values both for equivalent diameters and for thicknesses, which were independent of the formation ages and temperatures. Growth spirals were observed commonly on the basal surfaces of illite crystals. These data indicate that spiral growth operated as a growth-controlling process for the Ostwald ripening, which occurred during the late stages of illitization. However, the normalized particle-size distribution curves fitted to a log-normal distribution curve better than the theoretical profile calculated for a screw-dislocation model by Chai (1975), as found by Eberl et al. (1990). The ripening illite crystals changed in morphology from laths to hexagons while they grew at a constant ratio of particle diameter to thickness (approximately 40), as was estimated from the mean volume and area of the particles. The ratio is consistent with the measured ratio of step separation to step height of the growth spirals. This morphological evolution forms a trend on a plot of mean diameter vs. mean aspect ratio that is distinct from a trend delineated for illitic minerals from diagenetic shales and bentonites. The difference in trends may be related to differences in the growth rate of illite crystals during ripening among various rock types. The most likely factor controlling the growth rate of illite crystals during ripening might be variations in the level of supersaturation with respect to illite in the pore solution by advective solute flux from outside of the system. In the rocks associated with a high-porosity, fluid-dominated system, such as hydrothermally altered pyroclastics from Kamikita, a percolating flow may facilitate growth of larger illite crystals during ripening, which would result in a coarsely skewed particle size distribution, as found in this study.

Introduction

The conversion of smectite to illite occurs during burial diagenesis, hydrothermal alteration, and contact metamorphism. During this reaction, the proportion of smectite or of expandable layers in interstratified illite-smectite (I/S) decreases as functions of temperature, time, and chemical variables (e.g., Środoń and Eberl, 1984). However, the mechanism and kinetics of this reaction are not well understood. Variations in the morphology of I/S crystals, studied by transmission and scanning electron microscopy (TEM and SEM), indicate that smectite dissolves and illite recrystallizes in high-porosity, fluid-dominated (HPFD) systems, such as hydrothermally altered pyroclastics and diagenetically altered sandstones (Nadeau et al., 1985; Pollastro, 1985; Keller et al., 1986; Inoue, 1986; Inoue et al., 1987, 1988, 1992; Whitney, 1990; Altaner, 1989). A dissolution and recrystallization mechanism also was indicated by drastic changes in O isotopes during the illitization of smectite in laboratory experiments (Whitney and Northrop, 1988). Additionally, the measurement of particle diameters and particle thickness distributions indicated that recrystallization or coarsening proceeds by Ostwald ripening (Inoue et al., 1988; Eberl and Środoń, 1988; Eberl et al., 1990). More recently, Lanson and Champion (1991) and Eberl (1993) showed that Ostwald ripening occurs during the later stages of illitization during shale diagenesis, which is characterized as a low-porosity, rock-dominated (LPRD) system by Whitney (1990). The cited works suggested that an understanding of the growth processes of illite during Ostwald ripening may provide important information that could be used to model the dynamics of illite formation.

The present study has been undertaken first to characterize quantitatively the morphology of illite and I/S from an HPFD hydrothermal system and includes measurements of crystal habits, particle size distributions, and surface microtopographies. Second, a comparison was made between these morphologies and those formed during the smectite to illite conversion in LPRD systems.

0003–004X/94/0708–0700$02.00

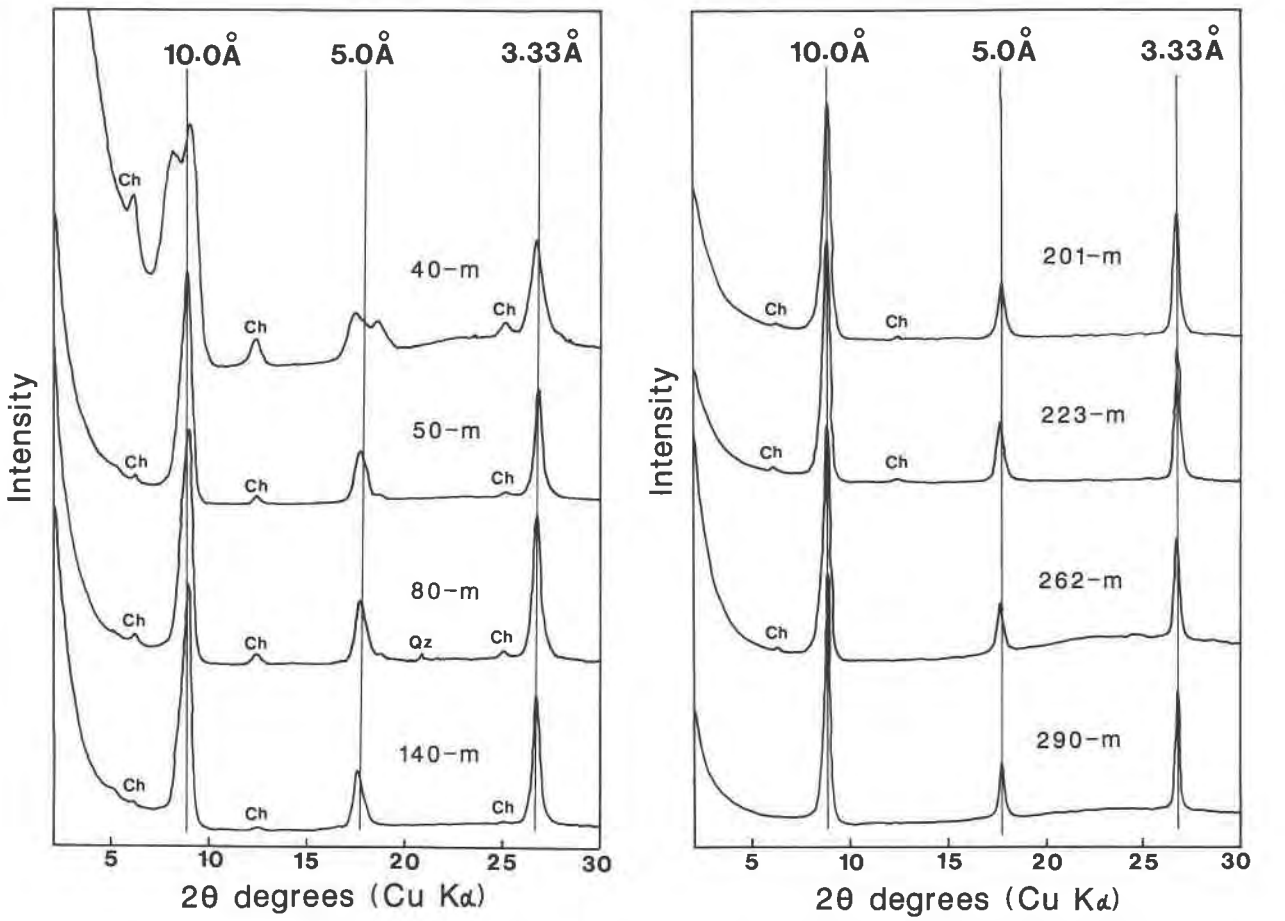

Fig. 1. X-ray powder diffraction patterns of glycolated samples from the Kamikita hydrothermal system. Ch = chlorite, Qz = quartz.

Samples and experimental methods

Samples

Eight samples of I/S and illite from drill hole no. 12 in the Kamikita hydrothermal alteration area (Aomori Prefecture, Japan) were used in this study (Table 1). K-Ar chronological and petrographic studies of many drill holes from this area distinguished four types of alteration that occurred at different times (Inoue and Utada, 1991). Among them, the occurrence of systematic smectite to illite conversion is restricted to the alteration related to the Kuroko mineralization during the Miocene (Inoue and Utada, 1991; Inoue et al., 1992). According to optical microscopic observation of thin section of the core samples, the original rocks were dacitic lavas and pyroclastics. The rocks were intensively altered to I/S, illite, chlorite, quartz, and sporadic barite, and occasionally they contain younger veinlets of siderite. The formation temperatures ranged from approximately 150 to 250 °C, as deduced from mineral assemblages (Inoue and Utada, 1991).

Methods

The original rock samples were crushed gently in an agate mortar and dispersed in distilled H_2O by using an ultrasonic vibrator, and then the <2-μm fraction was separated from the dispersed solution by centrifugation. The separated clay samples often contained a significant amount of chlorite, which is undesirable for TEM observation. High-gradient magnetic separation (at 2 T) (Righi and Jadault, 1988) was carried out on the chlorite-rich samples for 4–5 h. As shown in Figure 1, small amounts of chlorite still remained in some samples; the maximum

Table 1. Percent of expandable layers, *Ir* values, Kubler indexes, 2*M*, content, and K-Ar age of Kamikita illitic materials

Sample	Expandable layers (%)	*Ir* values	Kubler index (°)	2*M*, content (%)	K-Ar age (m.y.)
12-40-m	12	4.21	1.20	0	10.7(0.5)
12-50-m	3	1.30	0.65	10	11.8(0.6)
12-80-m	4	1.19	0.75	5	11.6(0.6)
12-140-m	3	1.21	0.70	13	11.5(0.6)
12-201-m	0	1.20	0.58	20	12.0(0.6)
12-223-m	0	1.11	0.51	30	11.3(0.6)
12-262-m	0	1.01	0.43	32	11.9(0.6)
12-290-m	0	1.12	0.35	25	12.4(0.6)

Note: values in parentheses indicate the standard deviation values of K-Ar age determination.

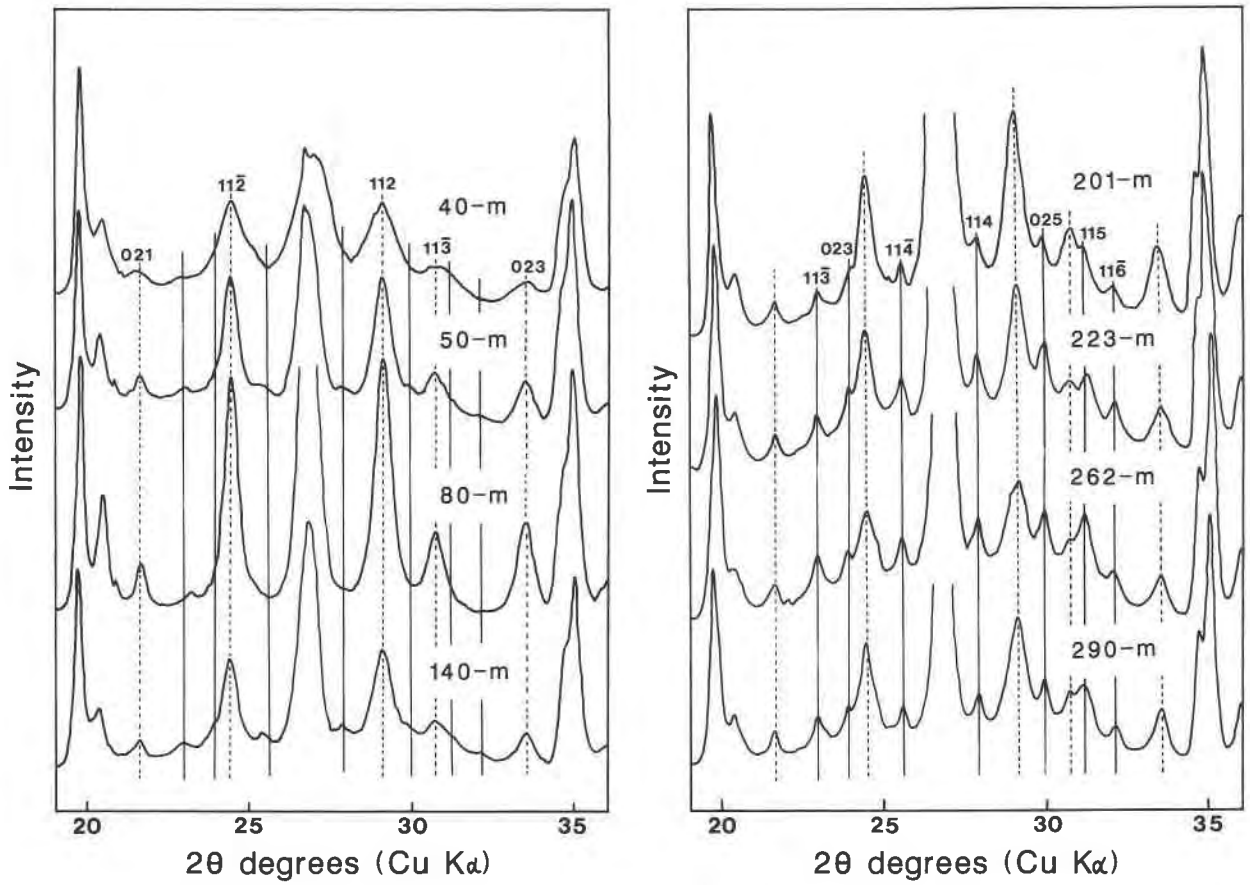

Fig. 2. X-ray powder diffraction patterns of Kamikita illitic materials measured in random preparations. The dashed and solid lines trace the peak positions indexed on the basis of $1M$ and $2M_1$ unit cells of mica, respectively.

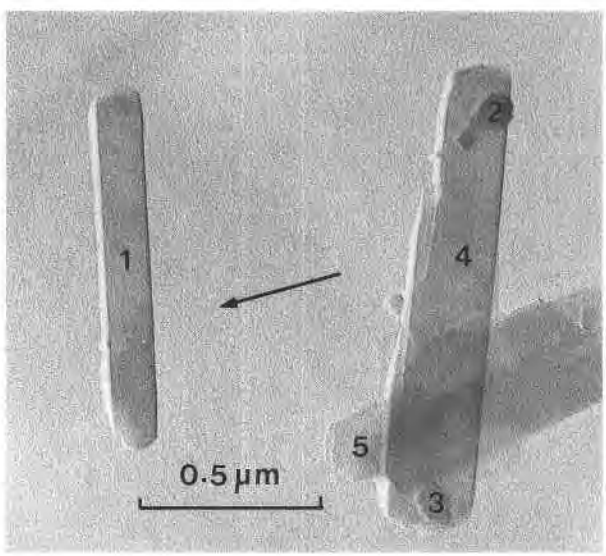

Fig. 3. Example (140-m sample) of three-dimensional size measurement of particles by a Pt-shadowing technique. Particles 1, 2, and 3 are selected for three-dimensional size measurement. Only length and width are measured on particle 4. Particle 5 is not measurable. The arrow indicates the shadowing direction.

amount was approximately 10% in the 40-m sample, which was estimated by semiquantitative X-ray diffraction (XRD) analysis. No dispersing agent was used throughout the preparation.

The percentage of expandable layers in illitic minerals was determined by comparing the observed XRD patterns (Fig. 1) with computer-simulated patterns using a Newmod program (version 2.3, developed by R. C. Reynolds, Dartmouth College, Hanover, New Hampshire). XRD patterns of randomly oriented specimens (Fig. 2) show the Kamikita samples to be mixtures of $1M$ and $2M_1$ polytypes having variable proportions. The $2M_1/(2M_1 + 1M)$ ratio was determined by a comparison of XRD intensity between 11$\bar{2}$ or 112 peaks for $1M$ and 11$\bar{4}$ or 114 peaks for $2M_1$ (Togashi, 1979; Mukhamet-Galeyev et al., 1985).

For TEM examination, a droplet of diluted suspension from each sample after high-gradient magnetic separation treatment was deposited on a C-coated collodion grid. The proper concentration of clay suspension needed to obtain a good dispersion on the grid was determined by trial and error. After drying at room temperature, the TEM grids were Pt-Pd shadowed at a known angle of about 20°. The length (L), the width (W), and the shadow

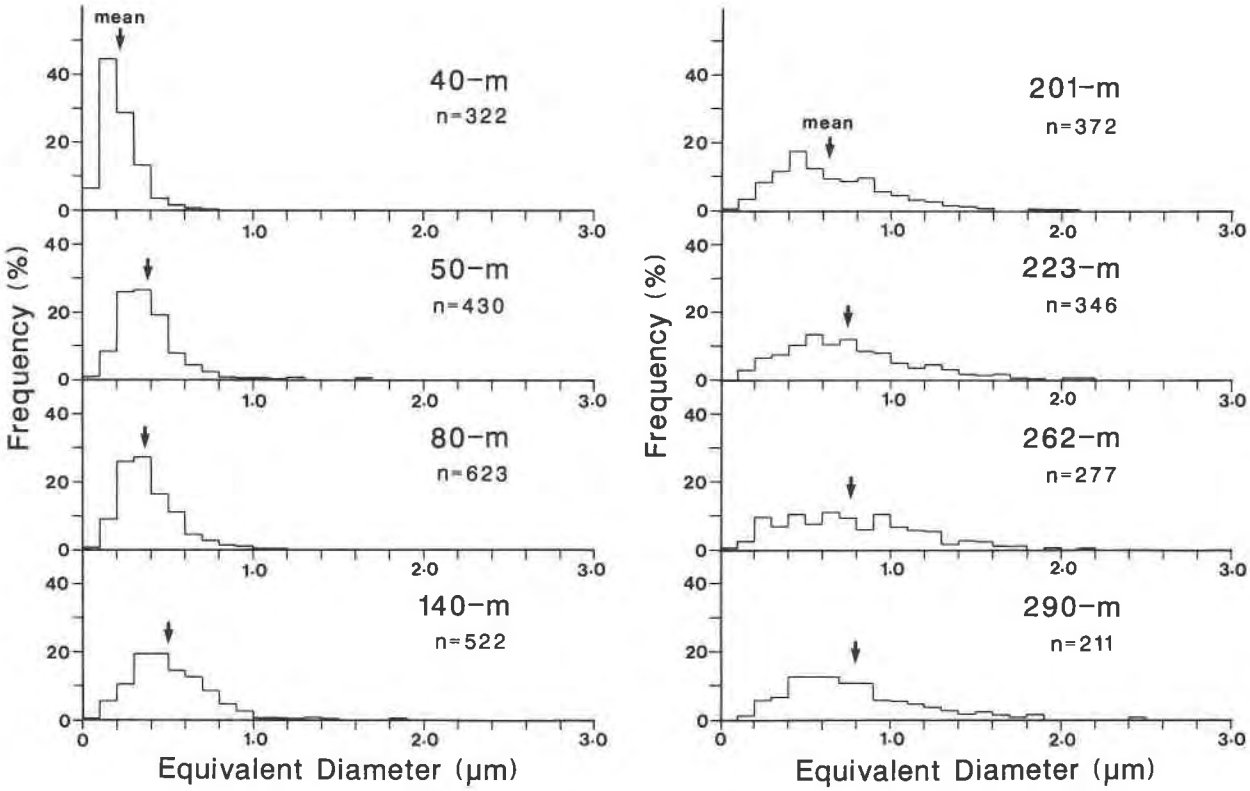

Fig. 4. Histograms of equivalent diameter for the Kamikita illitic materials at different depths. Arrows indicate the mean values. The *n* indicates the number of particles measured.

breadth of apparently individual particles were measured on TEM photographs, as described by Inoue et al. (1988). The thicknesses (T) of individual particles were calculated using the measured shadow breadth, the shadowing angle, and the magnification. The measurement error on the photographs was ±0.05 mm for each dimension; the final uncertainty is estimated to be ±2 nm for L and W and ±0.5 nm for T. In this study, the length and width of a particle are defined as the greatest and smallest distances of regular form, as shown in Figure 3. The L and W values defined here are slightly greater than those used by Lanson and Champion (1991) but are the same as those used by Nadeau (1985, 1987).

The equivalent circular diameter [$D = 2(LW/\pi)^{0.5}$], the aspect ratio ($R = L/W$), the area ($A = LW$), and the volume ($V = LWT$) were calculated for each particle. The D value defined in this study is different from both the equivalent square diameter [$D = (LW)^{0.5}$] used by Nadeau (1985, 1987) and that defined by Lanson and Champion (1991), who calculated it from the axes of an ellipse inscribed in each particle's convex outline (the detailed method is described in Champion, 1989). Values for D were recalculated from Nadeau's data in order to compare the D values of illite from different rock types.

Experimental procedures for the Au decoration were similar to the techniques adopted by Kitagawa et al. (1983) and Kitagawa and Matsuda (1992).

The K-Ar age determination of clay fractions (<2 μm) was carried out by Teledyne Isotope Company Limited (Table 1). The K_2O contents ranged from 3.2 wt% in the

Table 2. Mean for length, width, equivalent diameter, and aspect ratio, and area of particles in the Kamikita illitic materials

Sample	Particles measured	Length (μm)	Width (μm)	EQD (μm)	Ratio	Area ($nm^2 \times 10^4$)
12-40-m	322	0.396(0.272)	0.101(0.054)	0.222(0.110)	4.041(2.743)	3.08
12-50-m	430	0.695(0.499)	0.193(0.121)	0.395(0.210)	3.991(2.609)	9.77
12-80-m	623	0.663(0.385)	0.184(0.086)	0.382(0.169)	3.841(2.050)	9.48
12-140-m	522	0.742(0.394)	0.287(0.149)	0.505(0.226)	2.864(1.586)	16.22
12-201-m	372	0.885(0.487)	0.387(0.216)	0.645(0.322)	2.449(1.140)	25.35
12-223-m	346	0.984(0.503)	0.465(0.259)	0.749(0.369)	2.316(1.324)	33.81
12-262-m	277	0.967(0.524)	0.505(0.286)	0.773(0.395)	2.097(1.002)	34.67
12-290-m	211	0.985(0.563)	0.517(0.314)	0.789(0.434)	2.146(1.145)	37.76

Note: standard deviations are given in parentheses.

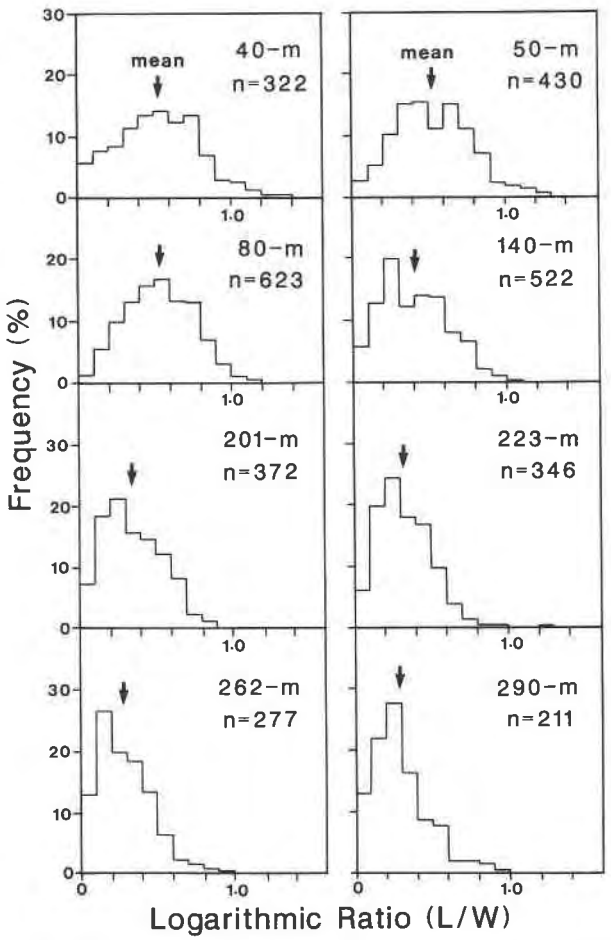

Fig. 5. Histograms of logarithmic aspect ratio for the Kamikita illitic materials at different depths. Arrows indicate the mean values.

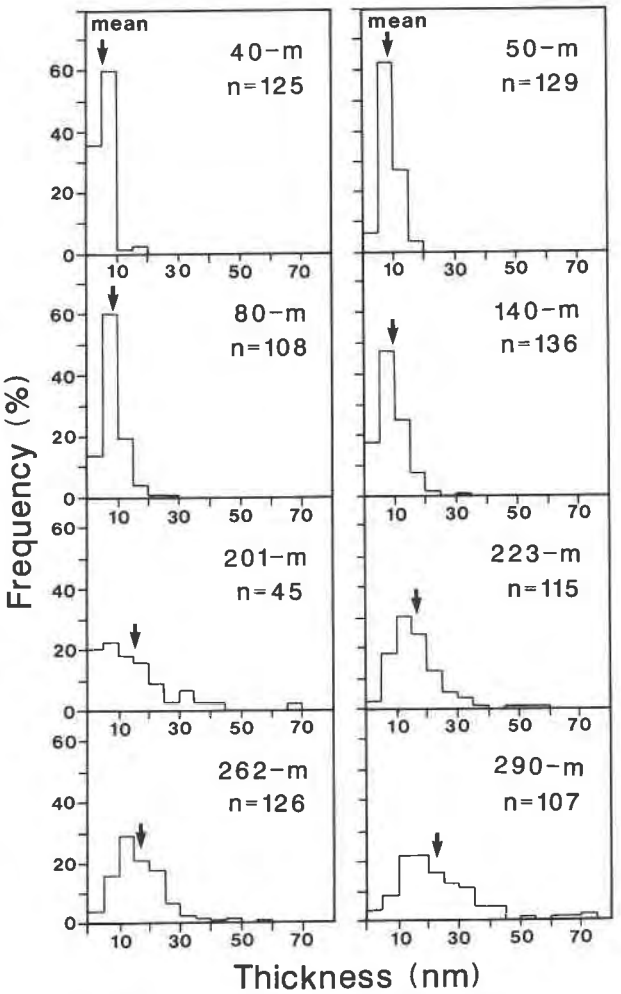

Fig. 6. Histograms of thickness for the Kamikita illitic materials at different depths. Arrows indicate the mean values. The *n* indicates the number of particles measured.

40-m sample to 7.9 wt% in the 223-m sample. The uncertainty ranged from 0.5 to 0.6 m.y.

Experimental results

XRD analysis

The percentage of expandable layers in the Kamikita samples ranges from 12 to 0 and decreases with depth and K-Ar age (Table 1). Środoń (1984) introduced an XRD peak-intensity ratio, *Ir* [$Ir = (001/003_{\text{air-dried}})/(001/003_{\text{glycol}})$], to detect small amounts of expandable layers in I/S. The estimated percentage of expandable layers in Table 1 were almost equal to those calculated from the *Ir* values (Table 1), according to a calibration curve given by Eberl et al. (1987). The Kubler index (full width in degrees 2θ at half height of the 001 peak), measured as defined by Eberl and Velde (1989), is given in Table 1 for comparison.

The 40-, 50-, 80-, and 140-m samples (Fig. 2) display peaks typical of the $1M$ polytype of mica, and the 40-m sample, $1M_d$, is slightly disordered, according to the criteria of Yoder and Eugster (1955). The samples at depths from 201 to 290 m contain a significant amount of illite-$2M_1$ in addition to -$1M$. The $2M_1/(2M_1 + 1M)$ ratio ranges from 0 to 0.32 and is highest in the 262-m sample (Table 1).

TEM examination

Figure 4 shows the histograms of frequency of equivalent diameter (D) as a function of depth. The histograms show asymmetrical distributions skewed toward larger diameters. The diameter distribution becomes broader with increasing depth, parallel to the decrease in the percentage of expandable layers in samples. The mean diameter calculated increases from 0.222 μm for the 40-m sample to 0.789 μm for the 290-m sample (Table 2).

Figure 5 presents the histograms of frequency of the log of the aspect ratio (log R) as a function of depth. The 40-m sample shows a wide range of distribution, from 1.335 to 0.01 in log R (from 21.6 to 1.02 in R), and the mean value of R is 4.04 (Table 2). I/S particles in the 40-m sample are laths elongated along the crystallograph-

Fig. 7. Examples of spiral patterns observed on the surface of Kamikita illitic materials; (**a**) illite-1*M* in the 80-m sample, (**b**) illite-1*M* in the 262-m sample, and (**c**) illite-2*M* in the 262-m sample.

←

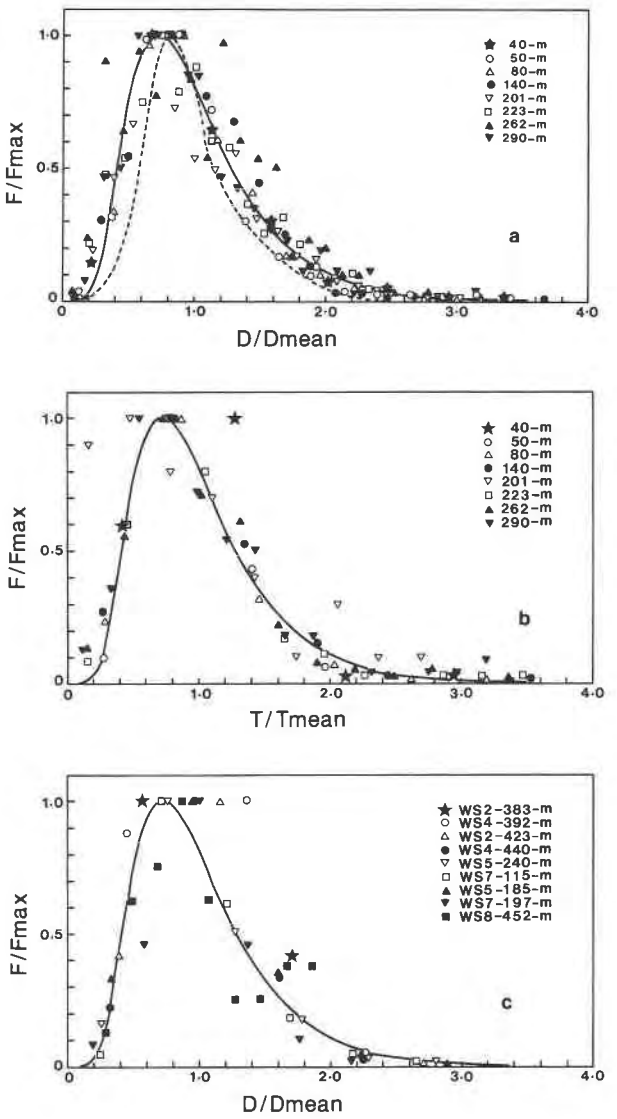

Fig. 8. (**a**) Equivalent diameter of Kamikita illitic materials normalized to the mode. The solid and dashed curves are a reduced profile calculated for the log-normal distribution curve and the theoretical curve of the screw-dislocation model calculated by Chai (1975), respectively. (**b**) Thickness of Kamikita illitic materials normalized to the mode. The solid line indicates the log-normal distribution curve calculated by using the same mean (α) and variance (β^2) values as those for the equivalent diameter in **a**. (**c**) Equivalent diameter of Shinzan illitic materials normalized to the mode. The solid line indicates the log-normal distribution curve calculated by using the same mean (α) and variance (β^2) values as those for the equivalent diameter of Kamikita illitic materials in **a**.

Table 3. Mean thicknesses and volume of particles in the Kamikita illitic materials

Sample	Particles measured	Thickness (nm)	V ($nm^3 \times 10^4$)
12-40-m	125	5.9(2.4)	18.17
12-50-m	129	8.9(3.1)	86.95
12-80-m	108	8.6(4.1)	81.53
12-140-m	136	9.2(4.6)	149.22
12-201-m	45	15.8(13.0)	400.53
12-223-m	115	16.6(9.1)	561.25
12-262-m	126	17.1(9.2)	592.86
12-290-m	107	22.7(13.3)	857.15

Note: standard deviations are given in parentheses.

ic **a** axis, as determined by a TEM diffraction technique. The aspect ratio distribution becomes asymmetrical and sharp and shifts toward smaller values with increasing depth. The mean R value of the 290-m sample is 2.15 (Table 2). Hexagonally shaped particles were commonly observed in the deeper samples.

Figure 6 shows the variation of thickness (T) as a function of depth. The histogram changes from a sharp and narrow distribution for the 40-m sample to a broad and flat one for the 290-m sample. The mean thickness calculated increases from 5.9 nm for the 40-m sample to 22.7 nm for the 290-m sample (Table 3). The mean area (A) and volume (V) of particles are summarized in Tables 2 and 3, respectively.

Examples of surface microtopographs observed on the Au-decorated specimens are given in Figure 7. A variety of step patterns, e.g., polygonal, elongated, malformed, composite, etc., patterns that were highlighted by the preferential precipitation of Au along steps, was observed on the basal surfaces of illitic minerals. Elongated rectangular spiral patterns, which originated from either a single or a few dislocation points, were characteristic of those samples composed dominantly of the $1M$ polytype (at depths from 40 to 140 m), as shown in Figure 7a. The longest straight section of the steps is always parallel to [100]. The number of steps in the spirals on the basal surface of illite-$1M$ tends to increase with depth (Figs. 7a and 7b). In the samples that contain a significant amount of the $2M_1$ polytype (depths from 201 to 290 m), the spirals are characterized by a hexagonal form following the crystal morphology. They often exhibit interlacing patterns (Fig. 7c). These step patterns are interpreted as the growth spirals of the $1M$ or $2M$ polytype of illite, according to Baronnet (1972, 1976, 1980).

Interpretation

Normalized particle size distribution

As described above, the D and T values of illite crystals from Kamikita increase with decreasing percentage of expandable layers and increase with increasing depth, K-Ar age, and $2M_1$-polytype content, indicating that the illitic minerals have coarsened during the smectite to illite conversion as functions of temperature and time. If coarsening proceeds by Ostwald ripening, it can be detected by an indirect method in which the particle size distribution is normalized to the modes, for example, by plotting frequency normalized to maximum frequency for the ordinate and diameter normalized to the mean diameter for the abscissa, as shown in Figure 8. The normalized distribution forms a steady-state profile, which becomes independent of ripening time and initial particle size distribution at steady state (Lifshitz and Slyozov, 1961; Wagner, 1961; Chai, 1975; Baronnet, 1982, 1984).

Figure 8a shows the normalized distribution of particle diameter in the Kamikita samples. It is apparent that the shape of the plots is independent of time and temperature, and gives a steady-state distribution with a maximum at $D/D_{mean} = 0.7$–0.8, skewing to larger values, and almost vanishing at $D/D_{mean} = 2.5$–3.0. According to Hanitzsch and Kahlweit (1968, 1969), Chai (1975), and Baronnet (1982, 1984), the shape of a steady-state profile is indicative of the type of the growth-controlling mechanism. The TEM observations of Au-decorated specimens favor the spiral growth mechanism for the Kamikita illitic materials, as shown in Figure 7. Sun and Baronnet (1989) have shown unambiguously from growth rate measurements that the growth of $\{hk0\}$ faces of synthetic phlogopite is controlled by a screw-dislocation mechanism. Indeed, the profile in Figure 8a is similar to the curve calculated on the basis of Chai's (1975) growth model controlled by a screw dislocation, but there are significant deviations at the smallest and greatest sizes. Following Eberl et al. (1990), it was assumed that the steady-state profile of diameter distribution is approximated by a log-normal distribution curve (plots of data on log-normal probability paper provided almost linear curves for all the data). The best-fit curve, determined by a least-squares method, has $\alpha = -0.09$, $\beta^2 = 0.23$, where α is the mean of the logarithmic D/D_{mean} values and β^2 is the variance (solid curve in Fig. 8a).

The normalized distribution of particle thickness for the Kamikita samples is illustrated in Figure 8b. It is also evident that the thickness distribution provides a steady-state profile, which is nearly coincident with that of the diameter. That suggests that the coarsening process of illitic minerals at Kamikita proceeds by Ostwald ripening and, in addition, that it occurs in the same manner both in the directions perpendicular to and within the **ab** plane of the illite crystals.

Figure 8c shows diameters of I/S and illite from the Shinzan hydrothermal system, recalculated from the data of Inoue et al. (1988). Surprisingly, the best-fit curve to the D and T data of Kamikita samples appears to be applicable to the diameter distribution of Shinzan illitic materials. Growth spirals, similar to those on the Kamikita samples, were observed on the basal surfaces of the Shinzan illitic minerals (Kitagawa, unpublished data). The best-fit curve obtained in the present study is not too different from the coherent domain-size distribution of hydrothermal illite obtained from XRD data by Eberl et al. (1990) and from the particle-diameter distribution of diagenetic illite given by Lanson and Champion (1991). Although Baronnet (1982) has shown from his autoclave

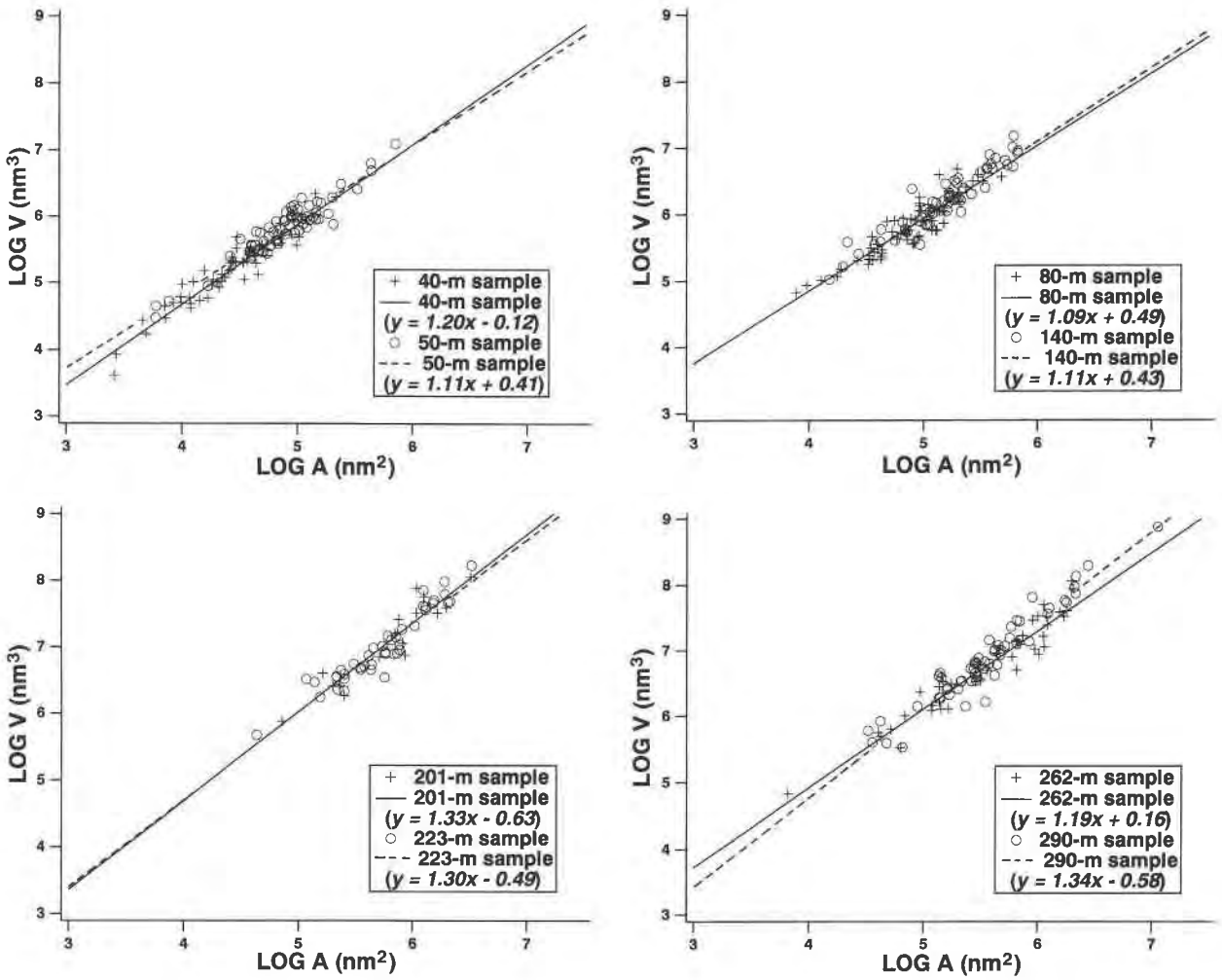

Fig. 9. Relationship between logarithmic area and volume of particles in Kamikita illitic materials at different depths. The lines indicate the best-fit equations.

experiments that the normalized size-distribution curve for phlogopite crystals grown by a spiral growth mechanism agrees almost perfectly with the theoretical profile calculated for a screw-dislocation model by Chai (1975), the present study seems to support the hypothesis that the particle size distribution of illite crystals formed by a spiral growth mechanism during Ostwald ripening is approximated by a log-normal distribution, as found by Eberl et al. (1990). As well as in the case of natural illitic minerals, log-normal distributions have been observed for most particulate materials, such as other minerals, metals, and snow (Colbeck, 1987; Eberl et al., 1990). No one has yet succeeded in matching experimental log-normal particle size distributions with theory. Colbeck (1987) noted as problematic that Ostwald-ripening processes lead to a log-normal size distribution.

Relation between area and volume of particles

Nadeau (1987) has shown that a good correlation exists between the mean volume and area of particles in micaceous clay minerals, including sericites, illites, and natural and synthetic I/S minerals. The log V vs. log A plots of data from the Kamikita samples are given in Figure 9. A positive correlation is evident between the area and the volume of particles for each sample, suggesting that a simple geometrical relation is obeyed in growing illite particles. If the slope of a log V vs. log A plot in Figure 9 is 1.0, the volume of particles increases with increasing area at a constant thickness during growth (see Fig. 10). If the growth takes place with increasing thickness at a constant area, the log V vs. log A plot exhibits a straight line parallel to the volume axis. In fact, the slopes determined by the least-squares method range from 1.09 to 1.20 for the samples at depths from 40 to 140 m and from 1.19 to 1.34 for the samples at depths from 201 to 290 m. These values of slope indicate that the growth of illite at Kamikita is due to a spiral mechanism rather than to a two-dimensional layer by layer mechanism. The numerical distinction in slope is related to the content of the $2M_1$ polytype in the samples; the samples containing

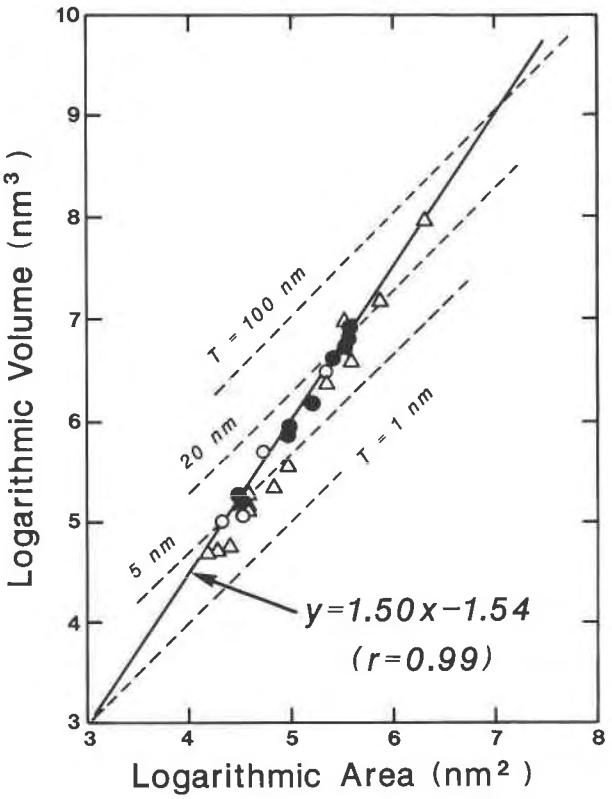

Fig. 10. Relationship between logarithmic mean area and volume in illitic minerals, including solid circles = Kamikita samples (this study), open circles = Inoue et al. (1988), triangles = Nadeau (1987). The solid line indicates the best-fit equation for the Kamikita samples. The dashed lines indicate a constant thickness (T) for 1, 5, 20, and 100 nm.

a significant amount of illite-2M_1 show relatively greater slope values than those in the samples dominantly comprising the 1M polytype.

To characterize quantitatively the morphological evolution associated with the growth process of illitic minerals at Kamikita, the logs of the mean values of volume and area for each sample are plotted in Figure 10, following Nadeau (1987). The relation log V vs. log A is described by the equation: $\log V = 1.50 \log A - 1.54$ (correlation coefficient $r = 0.99$). The equation can be easily converted to the relation between the thickness and the area of the particles: $T = (1/34.7)(A)^{0.5}$. In turn, the ratio of diameter to thickness is 39.2 for the Kamikita samples, since $A = \pi D^2/4$. The calculation shows that, on average, the Kamikita illitic minerals grew at a constant D/T ratio of approximately 40. By comparison, the D/T value for all the illite data, plotted in Figure 10, including data from Nadeau (1987) and Inoue et al. (1988), is slightly larger (i.e., $D/T = 57.1$).

If the growth process of illite at Kamikita proceeds by a spiral growth mechanism, the geometrical ratio D/T of a particle can be related to the ratio of step separation (λ) to step height (h) of growth spirals appearing on the basal surface. As a first approximation, consider an ideal Archimedean spiral developed from the emergence of a screw dislocation at P on the crystal depicted in Figure 11. In such a case, $D/T \leq \lambda_0/h$, where λ_0 and h are the step separation and step height, respectively. Here, H is the thickness of the crystal body that remains after subtracting the portions of the spirals at the top and bottom. If H is zero, $D/T = \lambda_0/h$ and D/T becomes smaller than λ_0/h with increasing H. In other words, if a crystal is very thin, λ_0/h is close to D/T. Figure 12 shows the measured distances between the arms of the spiral in two samples. The mean λ_0/h ratios were calculated to be 37.8 and 52.2 in the 80- and 262-m samples, respectively, assuming that the height of a step in illite-1M or -2M is a polytype repeat distance. The values are close to the geometrical ratio of $D/T = 40$ obtained from the previous particle size measurement. Of course, these values are within the range of values, 10^1–10^3, reported by Sunagawa et al. (1975), Kitagawa et al. (1983), and Tomura (1985) for the ratio of step separation to step height in muscovite and illite from natural hydrothermal systems.

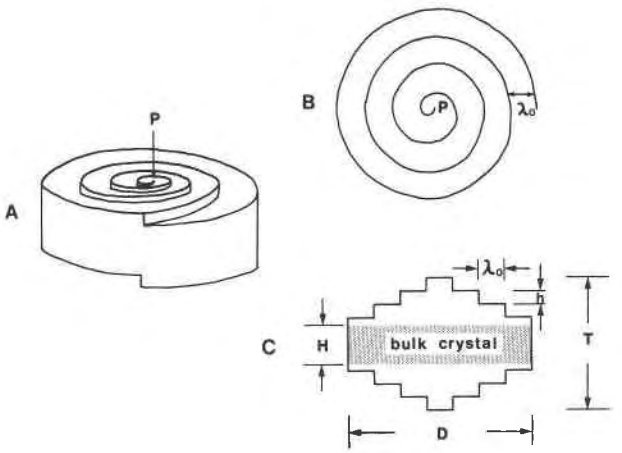

Fig. 11. Schematic drawing of a hypothetical Archimedean spiral viewed from various directions: (**A**) an overview, (**B**) a top view, (**C**) a side view.

The morphological evolution of illite in different rock types

Figure 13 is a plot of the mean particle diameter and the logarithmic mean aspect ratio of illitic minerals from different rock types. In the Kamikita samples, again, I/S having 12% of expandable layers from the 40-m sample occurs as thin laths elongated in the **a**-axis direction. The mean values of diameter and aspect ratio are 0.222 μm and 4.04 (Table 2). During the coarsening process, the I/S particles did not continue to grow as elongated crystals but rather as equidimensional forms similar to hexagons. For example, the mean diameter and aspect ratio are 0.789 μm and 2.15 in the 290-m sample (Table 2). This variation in morphological evolution provides a unique trend on the diagram. Hydrothermal illitic minerals from Shinzan (Inoue et al., 1988), the original rocks of which are similar to those in Kamikita, appear to scat-

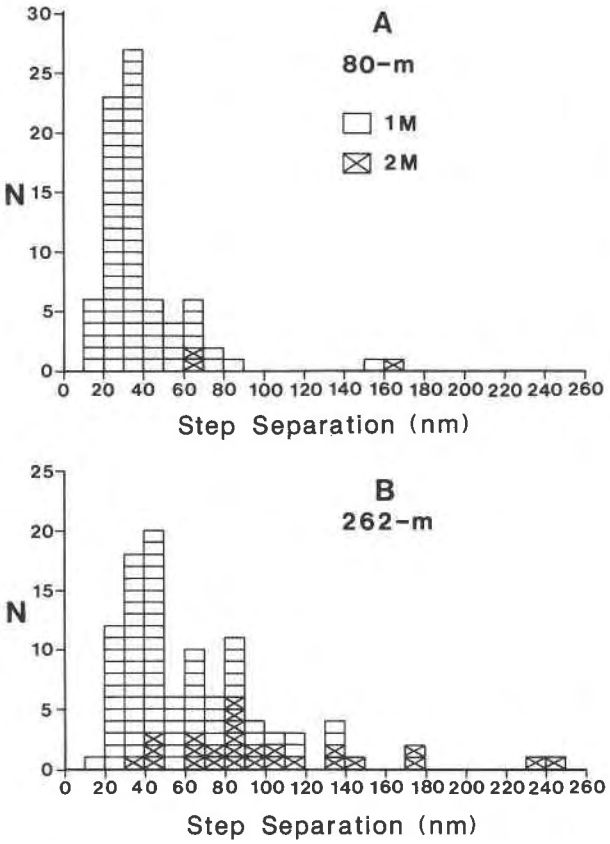

Fig. 12. Histograms of the step separation of spirals in (**A**) 80-m and (**B**) 262-m samples.

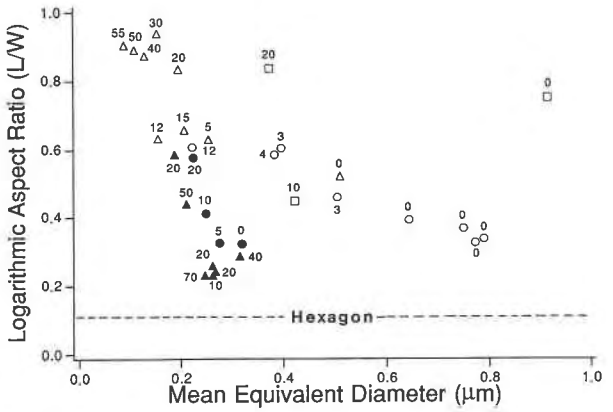

Fig. 13. Plots of logarithmic mean aspect ratio vs. mean equivalent diameter of illitic materials from various rock types. Open circles = the Kamikita hydrothermal system (this study), open triangles = the Shinzan hydrothermal system (Inoue et al., 1988), solid triangles = diagenetic bentonites (Nadeau, 1985), closed circles = diagenetic shales (Lanson and Champion, 1991), open squares = diagenetic sandstones (Nadeau, 1985). Numerical figures indicate the percentage of expandable layers.

ter along the same trend as the Kamikita samples (Fig. 13). The trend for the two hydrothermal samples is described approximately by the following relation: $\log R = 0.903 - 0.771D$ (the curve is not shown in the figure), in the range from about 50 to 0% expandable layers. Illitic minerals from diagenetic sandstones (Nadeau, 1985) apparently tend to scatter along the hydrothermal trend, though with great deviation. On the other hand, when the data of I/S and illite from diagenetic shales (Lanson and Champion, 1991) and from diagenetic bentonites (Nadeau, 1985) are plotted on the diagram, they give a different trend: a cluster of points scattering within the area delineated by smaller values of R and D, without regard for their percentage of expandable layers.

The rock types plotted in Figure 13 are considered to represent those in the HPFD and LPRD systems, according to Whitney (1990); hydrothermally altered pyroclastics and diagenetically altered sandstones are rocks in the HPFD systems, and diagenetically altered shales and bentonites are those in the LPRD systems. The duration of the smectite to illite conversion ranged from 1 to 2 m.y. in the Kamikita (this study) and Shinzan (Inoue et al., 1992) hydrothermal systems. Although the K-Ar ages of the diagenetic samples cited are not reported, it may be assumed that the smectite to illite conversion occurred over longer times in diagenetic environments. It has been demonstrated that the samples in Figure 13, except Nadeau's samples, have undergone Ostwald ripening. It is also known that the illite crystals grew by the spiral growth mechanism at Kamikita and Shinzan. When one takes into account these assumptions, the two distinct trends in morphological evolution depicted in Figure 13 may be related to differences in the growth rate of illite crystals during Ostwald ripening between the HPFD and LPRD systems.

At a constant temperature, the overall growth rate of a crystal is described on the basis of a simple power-law relationship according to Baronnet (1982): $R = K\sigma^n$, where R is the overall growth rate of crystal, K is the kinetic coefficient, σ is the relative supersaturation, and n is the order of the kinetics. Second-order kinetics, i.e., $n = 2$, operates in the spiral growth processes under low-supersaturation conditions. According to Baronnet (1982), the growth rate of illite crystals during Ostwald ripening may be affected by many factors, such as temperature, chemical variables, rock porosity, flow rate of solution, etc. It is known that the smectite to illite conversion occurs within a similar range of temperatures in varied systems (Środoń and Eberl, 1984). At a fixed temperature, the kinetic coefficient, K, is generally assumed to be constant if the other variables remain unchanged during ripening. Thereby the effect of temperature may be ignored. Huang (1990) and Small et al. (1992) noted from their experimental studies on illite morphology that fibrous illite is favored by high silica activity in solution. This factor may explain the presence of long lath-shaped illite in diagenetic sandstones. From the growth rate equation, it is obvious that the growth rate increases with increasing supersaturation at a constant temperature. It is assumed that the Ostwald ripening occurs at relatively low supersaturation with respect to illite in the pore solution. However, a slight increase in the level of supersaturation dur-

ing ripening, even if it is small, can result in a significant increase in the growth rate of illite because the growth rate is a function of supersaturation to the second power. Since the Ostwald ripening is a diffusion-controlled process, factors such as solute flux, flow rate, and H_2O-rock ratio influence the growth rate of illite through modifying the level of supersaturation at the crystal-solution interface. For example, flowing solution promotes the growth rate of illite (Baronnet, 1982). Furthermore, solute flux from outside of the system can modify the growth rate of ripening illite crystals. It would be expected that advective flux exists in the HPFD systems, whereas diffusional flux dominates in the LPRD systems (Whitney, 1990). Here, we assume a continuum between advective and diffusional fluxes. In the LPRD systems limited to the solute flux from outside, similar to a closed system, the growth rate decreases with increasing crystal size, as predicted by the theory of Ostwald ripening (Lifshitz and Slyozov, 1961; Wagner, 1961), and the ripening ceases at a finite time because of the limit of crystallizable mass in the system. Additionally, although illite crystals can grow until each crystal is impinged, rocks in the LPRD systems do not provide free space for growing illite. The resulting particle size of illite crystals increases to a limited extent in the LPRD systems. On the other hand, in the HPFD systems open to the solute flux, the level of supersaturation with respect to illite in the pore solution would be expected to be kept nearly constant during ripening, owing to continual advective flux. Such a situation allows the original growth rate of ripening illite crystals to remain constant for longer times, and the growth rate does not decrease as the size increases. The resultant particle size of illite becomes larger during ripening in the HPFD system. Additionally, the fact that the growth rate does not decrease as the size increases may cause the particle-size distribution to skew toward larger sizes (Colbeck, 1987), as found in this study. The assumption of a closed system plays an essential role in the classic theory of Ostwald ripening (Lifshitz and Slyozov, 1961; Wagner, 1961). However, recent theoretical studies have shown that the theory of Ostwald ripening is applicable to an open system (Beenakker and Ross, 1985; Nakahara et al., 1991). Consequently, the porosity and permeability of the rocks at the time when the ripening of illite took place are strongly related to the difference in the morphological evolution by the variation in the growth rate of illite crystals during ripening and to the resulting particle size distribution.

Acknowledgments

The authors gratefully thank D. Eberl, A. Baronnet, T. Nishida, M. Utada, S. Altaner, and G. Whitney for their valuable suggestions during the process of completing this study and for critical readings of the earlier versions of the manuscript. Critical reviews and comments by J. Środoń are gratefully acknowledged. The authors also wish to thank H. Tatematsu, Japan Railway Institute, for contributing the Kamikita samples. This study was financed in part by a grant in aid for scientific research from the Ministry of Education of Japan (no. 02640621/A.I.).

References cited

Altaner, S.P. (1989) Examination of models of smectite illitization. In Abstracts for the 26th Annual Meeting of Clay Minerals Society, Sacramento, California, 13.

Baronnet, A. (1972) Growth mechanisms and polytypism in synthetic hydroxyl-bearing phlogopite. American Mineralogist, 57, 1272–1293.

——— (1976) Polytypisme et polymorphisme dans les micas: Contribution à l'étude du rôle de la croissance cristalline, 256 p. Ph.D. thesis, Université d'Aix-Marseille III. Marseille, France.

——— (1980) Polytypism in micas: A survey with emphasis on the crystal growth aspect. In E. Kaldis, Ed., Current topics in material science, vol. 5, p. 447–548. North Holland, Amsterdam.

——— (1982) Ostwald ripening in solutions. The case of calcite and mica. Estudios Geológicos, 38, 185–198.

——— (1984) Growth kinetics of the silicates: A review of basic concepts. Fortschritte der Mineralogie, 62, 187–232.

Beenakker, C.W.J., and Ross, J. (1985) Theory of Ostwald ripening for open systems. Journal of Chemical Physics, 83, 4710–4714.

Chai, B.H.T. (1975) The kinetics and mass transfer of calcite during hydrothermal recrystallization process, 138 p. Ph.D. thesis, Yale University, New Haven, Connecticut.

Champion, D. (1989) Etude des mécanismes de transformation des interstratifiés illite/smectite au cours de la diagenèse, 204 p. Ph.D. thesis, Université de Paris–Sud, Centre d'Orsay, France.

Colbeck, S.C. (1987) Theory of particle coarsening with log-normal distribution. Acta Metallurgica, 35, 1583–1588.

Eberl, D.D. (1993) Three zones for illite formation during burial diagenesis and metamorphism. Clays and Clay Minerals, 41, 26–37.

Eberl, D.D., and Środoń, J. (1988) Ostwald ripening and interparticle-diffraction effects of illite crystals. American Mineralogist, 73, 1335–1345.

Eberl, D.D., and Velde, B. (1989) Beyond the Kubler index. Clay Minerals, 24, 571–577.

Eberl, D.D., Środoń, J., Lee, M., Nadeau, P.H., and Northrop, H.R. (1987) Sericite from the Silverton Caldera, Colorado: Correlation between structure, composition, origin, and particle thickness. American Mineralogist, 72, 914–934.

Eberl, D.D., Środoń, J., Kralik, M., Taylor, B.E., and Peterman, Z.E. (1990) Ostwald ripening of clays and metamorphic minerals. Science, 248, 474–477.

Hanitzsch, E., and Kahlweit, M. (1968) Zur Umlösung aufgedampfter Metallkristalle. I. Zeitschrift für physikalische Chemie neue Folge, 57, 145–155.

——— (1969) Zur Umlösung aufgedampfter Metallkristalle. II. Zeitschrift für physikalische Chemie neue Folge, 65, 290–305.

Huang, W.L. (1990) Illitic clay formation during experimental diagenesis of arkoses. In Abstracts for the 27th Annual Meeting of Clay Minerals Society, Missouri–Columbia, 62.

Inoue, A. (1986) Morphological change in a continuous smectite-to-illite conversion series by scanning and transmission electron microscopies. Journal of College of Arts and Sciences, Chiba University, B-19, 23–33.

Inoue, A., and Utada, M. (1991) Hydrothermal alteration in the Kamikita Kuroko mineralization area, Northern Honshu, Japan. Mining Geology, 41, 203–218.

Inoue, A., Kohyama, N., Kitagawa, R., and Watanabe, T. (1987) Chemical and morphological evidence for the conversion of smectite to illite. Clays and Clay Minerals, 35, 111–120.

Inoue, A., Velde, B., Meunier, A., and Touchard, G. (1988) Mechanism of illite formation during smectite-to-illite conversion in a hydrothermal system. American Mineralogist, 73, 1325–1334.

Inoue, A., Utada, M., and Wakita, K. (1992) Smectite-to-illite conversion in natural hydrothermal systems. Applied Clay Science, 7, 131–145.

Keller, W.D., Reynolds, R.C., and Inoue, A. (1986) Morphology of clay minerals in the smectite-to-illite conversion by scanning electron microscopy. Clays and Clay Minerals, 34, 187–197.

Kitagawa, R., and Matsuda, T. (1992) Microtopography of regularly-interstratified mica and smectite. Clays and Clay Minerals, 40, 114–121.

Kitagawa, R., Takeno, S., and Sunagawa, I. (1983) Surface microtopographies of sericite crystals formed in different environmental conditions. Mineralogical Journal, 11, 282–296.

Lanson, B., and Champion, D. (1991) The I/S-to-illite reaction in the late stage diagenesis. American Journal of Science, 291, 473–506.

Lifshitz, I.M., and Slyozov, V.V. (1961) The kinetics of precipitation from supersaturated solid solutions. Journal of Physics and Chemistry of Solids, 19, 35–50.

Mukhamet-Galeyev, A.P., Pokrovskiy, V.A., Zotov, A.V., Ivanov, I.P., and Samotoin, N.D. (1985) Kinetics and mechanism of hydrothermal crystallization of $2M_1$ muscovite: An experimental study. International Geology Review, 27, 1352–1364.

Nadeau, P.H. (1985) The physical dimensions of fundamental clay particles. Clay Minerals, 20, 499–514.

——— (1987) Relationships between the mean area, volume and thickness for dispersed particles of kaolinites and micaceous clays and their application to surface area and ion exchange properties. Clay Minerals, 22, 351–356.

Nadeau, P.H., Wilson, M.J., McHardy, W.J., and Tait, J.M. (1985) The conversion of smectite to illite during diagenesis: Evidence from some illitic clays from bentonites and sandstones. Mineralogical Magazine, 49, 393–400.

Nakahara, A., Kawakatsu, T., and Kawasaki, K. (1991) Ostwald ripening in open systems. Journal of Chemical Physics, 95, 4407–4417.

Pollastro, R.M. (1985) Mineralogical and morphological evidence for the formation of illite at the expense of illite/smectite. Clays and Clay Minerals, 33, 265–274.

Righi, D., and Jadault, P. (1988) Improving soil clay minerals studies by high-gradient magnetic separation. Clay Minerals, 23, 225–232.

Small, J.S., Hamilton, D.L., and Habesch, S. (1992) Experimental simulation of clay precipitation within reservoir sandstones. II. Mechanism of illite formation and controls on morphology. Journal of Sedimentary Petrology, 62, 520–529.

Środoń, J. (1984) X-ray diffraction of illitic materials. Clays and Clay Minerals, 32, 337–349.

Środoń, J., and Eberl, D.D. (1984) Illite. In Mineralogical Society of America Reviews in Mineralogy, 13, 495–544.

Sun, B.N., and Baronnet, A. (1989) Hydrothermal growth of OH-phlogopite single crystals. I. Undoped growth medium. Journal of Crystal Growth, 96, 265–276.

Sunagawa, I., Koshino, Y., Asakura, M., and Yamamoto, T. (1975) Growth mechanisms of some clay minerals. Fortschritte der Mineralogie, 52, 217–224.

Togashi, Y. (1979) Polytypes and expandability of sericite from the Itaya kaolin clay deposit, Northeast Japan. Journal of Japanese Association of Mineralogy, Petrology, and Economic Geology, 74, 100–113.

Tomura, S. (1985) Growth mechanisms and morphological variations of phyllosilicate crystals under different growth environments and conditions, 165 p. Ph.D. thesis, University of Tohoku, Tohoku, Japan.

Wagner, C. (1961) Theorie der Alterung von Neiderschlägen durch Umlösen (Ostwald Reifung). Zeitschrift für Electrochemie, 65, 581–591.

Whitney, G. (1990) Role of water in the smectite-to-illite reaction. Clays and Clay Minerals, 38, 343–350.

Whitney, G., and Northrop, H.R. (1988) Experimental investigation of the smectite to illite reaction: Dual reaction mechanisms and oxygen-isotope systematics. American Mineralogist, 73, 77–90.

Yoder, H.S., Jr., and Eugster, H.P. (1955) Synthetic and natural muscovites. Geochimica et Cosmochimica Acta, 8, 225–280.

Manuscript received October 5, 1992
Manuscript accepted February 16, 1994